

# Helminth defense molecules as design templates for membrane active antibiotics

*Katharine Hammond,<sup>1,2</sup> Helen Lewis,<sup>1</sup> Nilofar Faruqui,<sup>1</sup> Craig Russell,<sup>1</sup> Bart W Hoogenboom<sup>2,3</sup> and  
Maxim G Ryadnov<sup>1,4\*</sup>*

<sup>1</sup>National Physical Laboratory, Hampton Road, Teddington, TW11 0LW, UK

<sup>2</sup>Department of Physics & Astronomy, University College London, London, WC1E 6BT, UK

<sup>3</sup>London Centre for Nanotechnology, University College London, London, WC1H 0AH, UK

<sup>4</sup>Department of Physics, King's College London, Strand Lane, London WC2R

Corresponding author:

Dr Maxim G Ryadnov

National Physical Laboratory,

Hampton Road, Teddington, TW11 0LW, UK

Fax: (+44) 20 86140573

Tel: (+44) 20 89436078

max.ryadnov@npl.co.uk

**ABSTRACT:** a design template for membrane active antibiotics against microbial and tumor cells is described. The template is an amino-acid sequence that combines the properties of helminth defence molecules, which are not cytolytic, with the properties of host-defense peptides, which disrupt microbial membranes. Like helminth defence molecules, the template folds into an amphipathic helix in both mammalian host and microbial phospholipid membranes. Unlike these molecules, the template exhibits antimicrobial and anticancer properties that are comparable to those of antimicrobial and anticancer antibiotics. The selective antibiotic activity of the template builds upon a functional synergy between three distinctive faces of the helix, which is in contrast to two faces of membrane-disrupting amphipathic structures. This synergy enables the template to adapt pore formation mechanisms according to the nature of the target membrane, inducing the lysis of microbial and tumour cells.

**Keywords:** antibiotics, helminth defence molecules, antimicrobial peptides, membrane pore formation, atomic force microscopy, oncolytic agents

Uni- and multi-cellular infections successfully exploit host environments and manage host defence reactions. Bacteria secrete protein toxins that form small pores or channels in eukaryotic membranes causing the rapid discharge of vital resources (e.g. ions, ATP).<sup>1</sup> Multicellular parasites, such as helminths, infect tissues rather than cells and feed on nutrients that host cells absorb.<sup>2</sup> Pore formation mediated by bacterial toxins can lead to cell death, while nutrient supply disrupted by helminth infection weakens immunity. To elicit strong antimicrobial responses at the sites of infection, the immune systems of virtually all forms of life deploy host defence or antimicrobial peptides (AMPs).<sup>3</sup> These molecules are not necessarily specific, but sufficiently rapid to act within the time scales of their proteolytic stability.<sup>4</sup> Killing ensues via membrane pore formation, which favours microbial membranes without a strict predisposition for a particular architecture or size of resulting pores.<sup>5</sup> Poration mechanisms range from abundant pore formation to pore expansion and monolayer pits.<sup>6-8</sup>

Although bacteria may resist the action of these peptides by fortifying their cell surfaces, resistance mechanisms are not universal and can be counteracted by alterations in peptide structure.<sup>4,9</sup> A widespread resistance against AMPs remains challenging for microorganisms to develop and has yet to be reported.<sup>3,6</sup>

Unlike bacteria, helminths such as parasitic trematodes evade host defence by secreting a range of helminth defence molecules (HDMs).<sup>10</sup> These molecules benefit from interacting with host cells without the need to lyse them. Indeed, HDMs suppress inflammatory responses by specifically binding to host cells or by neutralising bacterial endotoxins before and after lysis.<sup>11</sup> This ability to exploit the innate immune system allows the molecules to support multiple biological functions. For example, HDMs can inhibit vacuolar ATPases leading to the impairment of antigen processing and display in macrophages<sup>12</sup> or prevent the activation of inflammasomes to interfere with immune-mediated metabolic and autoimmune disorders such as atherosclerosis and multiple sclerosis.<sup>13</sup>

Having no ability to disrupt cellular membranes, be these bacterial or host, HDMs yet share main structural characteristics with AMPs.<sup>14</sup> Both are cationic and can fold into amphipathic  $\alpha$ -helices. Effective AMPs can be designed with just two types of amino acids – cationic and hydrophobic, which upon folding cluster into two corresponding faces.<sup>5,15</sup> A generic selectivity to anionic microbial membranes can be achieved by keeping the ratio of cationic to hydrophobic residues at 3/2, whilst careful modifications of the cationic face with polar or small residues may help tune membrane disruption mechanisms.<sup>7,8</sup> HDMs have similar ratios of all polar to hydrophobic residues. This allows to avoid hemolytic effects that are characteristic of venomous or toxin peptides exhibiting more extended hydrophobic faces (e.g. melittin, pardaxin).<sup>15-17</sup> These structural similarities prompt further comparisons. In solution AMPs adopt random coil conformations that in microbial membranes convert to amphipathic secondary structures (i.e.  $\beta$ -sheets,  $\alpha$ -helices).<sup>3-5</sup> This is different from peptide toxins that are predominantly hydrophobic and fail to differentiate between microbial and zwitterionic mammalian membranes, folding in both.<sup>5, 16, 17</sup>

HDMs are anticipated to have the same ability to fold upon binding to microbial or mammalian membranes, or to both types. Yet, they do not disrupt them. This distinction challenges a seemingly necessary link between membrane-induced folding and biological activity. In addition, and, more importantly, it alludes to cryptic features in HDM structures that can be exploited for antimicrobial discovery. We base this reasoning on that both AMPs and HDMs are evolutionarily conserved sequences that successfully maintain their functional roles. Here we set out to establish that HDMs offer tuneable sequence templates that can bind to and fold on both host and microbial membranes, which are amenable to the design of gene-encoded antibiotics active against microbial and cancer cells.

## **Results and Discussion**

Our approach applies the principles of inverse protein folding to the design of antimicrobial amino-acid sequences. First of all, a design template must accommodate residues that are characteristic of AMPs at the ratios minimising non-specific toxicity. Many HDMs already meet this criterion. However, the relative ratio of cationic amino acids in their polar faces is low. This leads to another requirement: a folded template should incorporate additional cationic residues at the expense of neutral polar residues in the polar face. Such an arrangement splits the polar face into two polar facets (cationic and non-cationic) and combines non-cationic residues into a continuous polar seam running along the helix axis. Consequently, the non-cationic polar facet may expose a unique structural motif for membrane binding. We hypothesise that such a motif can be found in HDM sequences, is complementary to antimicrobial function and can provide an auxiliary biological property.

Based on these conventions, we identified and synthesized an autonomous amphipathic helix in an archetypal HDM that was originally isolated from *F. hepatica* and that closely mimics mammalian AMPs (Figs 1 and S1 in Supporting Information). This HDM, termed *F. hepatica* HDM 1 (FhHDM-1), is cleaved by an endopeptidase cathepsin L1 to release a C-terminal domain, which possesses all the properties characteristic of HDMs.<sup>14</sup> The domain, is dominated by a conserved amphipathic helix,

**1**. The helix incorporates structural features that are not typical of AMPs, but which we deemed unique in the context of membrane binding (Fig 1A).

Apart from having a well-defined hydrophobic face, **1** has a continuous non-cationic polar face (Fig 1B, C). Some cationic residues appear to alternate with hydrophobic residues near the polar face rather than cluster together into a distinctive facet. This property is common among membrane-active peptides and serves to acquire imperfect amphipathicity that helps the peptides better adapt to curved membranes. Three anionic residues in **1** are involved in stabilising  $i, i+3$  or  $i, i+4$  electrostatic interactions: these are likely to regulate the contributions of the cationic residues and also neutralise the overall net charge of the helix (Fig 1B). Because of these features, **1** is different from antimicrobial sequences that are characterized by the segregation of cationic residues into cationic faces. More notably, however, the helix of **1** has a cluster of threonyl residues that is placed between the hydrophobic and polar faces. Proteins are known to allocate threonine-rich amphipathic structures for sensing curvature and lipid packing in membranes.<sup>18</sup> These structures act as amphipathic lipid packing sensor (ALPS) motifs that support the dissociation of coat proteins thereby regulating membrane traffic from Golgi-derived membranes. Similarly, FhHDM-1 recognises lipid rafts on macrophages before being taken up by the host cell via an endosomal pathway, suggesting that the peptide has an ALPS-like function.<sup>12</sup> In addition, threonyl residues have the highest helical penalty among amino acids that are capable of adopting secondary structures. This may further support the importance of the cluster for FhHDM-1.

To exploit a synergistic role of the cluster in designing HDM-templated antibiotics, we converted **1** into a helminth antibiotic template, **2** (Figs 1 and S1). The resulting helix features the same hydrophobic face, but extended with an isoleucine replacing one of the arginyl residues that flank the valine in **1** (Fig 1B). A cationic face in **2** then continues with the remaining arginine followed by four consecutive lysyl residues (Fig 1B). This arrangement has two distinct seams running along the helix. The seams provide a clear separation from the remainder of the polar face, which was adjusted to host

the threonyl cluster (Fig 1C). A single seryl residue was used to replace a glutamate. This allowed to extend the cluster without introducing additional threonines. Serines are equally common for helical ALPS motifs, which they bend together with threonines at a small angle with respect to the helix axis.<sup>19</sup> Transmembrane helices with such bending angles more readily adopt conformational changes in membranes. Therefore, the threonyl cluster, being placed opposite to the cationic face in **2**, was anticipated to facilitate poration in membranes regulated by localised charge interactions. Finally, the neutral and polar asparaginy residue, which has the same helical penalty as threonine, but no preference for any of the faces, was kept in the original position to mark the separation between the cationic face and the threonyl cluster.

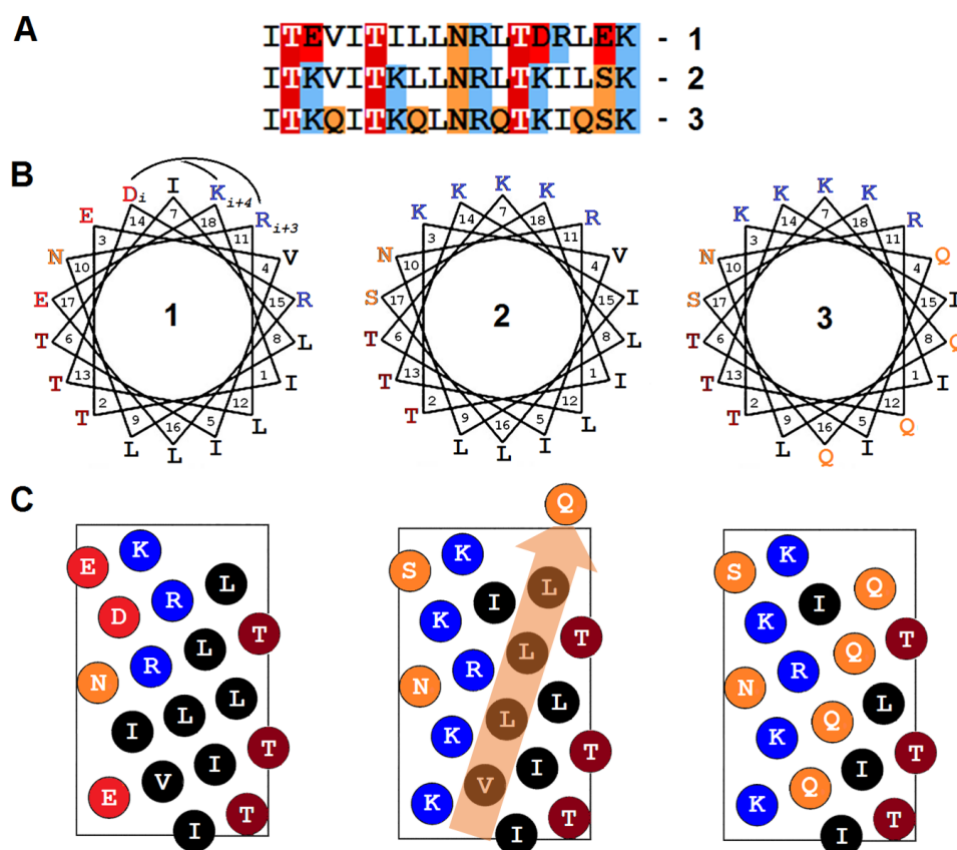


**Figure 1. Helminth antibiotic template.** Linear sequences (A) and configured onto helical wheels (B) and helical nets (C). The amino and carboxyl-termini of the sequences are free. Cationic, anionic and neutral polar residues are in blue, red and orange respectively. Curved arrows in B denote stabilising  $i, i+3$  and  $i, i+4$  electrostatic interactions. The orange arrow in C highlights the hydrophobic residues of **2** that were replaced with glutamines to create a helix breaking polar seam, giving rise to **3**.

Consistent with the design rationale, neither **1** nor **2** folded in solution at micromolar peptide chain concentrations: circular dichroism (CD) spectra revealed characteristic random coil conformations (Fig S2). By contrast, both peptides were appreciably helical in reconstituted unilamellar vesicles that mimicked anionic microbial and zwitterionic mammalian phospholipid membranes, respectively (Table S1). This is notable since AMPs do not tend to fold in zwitterionic membranes and lack threonyl clusters. To directly compare the observed behaviour with that of AMPs, the same tests were performed for cecropin B and magainin 2 – representatives from two major classes of naturally occurring AMPs.<sup>5</sup> These peptides were found to fold exclusively in anionic membranes (Fig S2). This is in accord with the selective folding of AMPs in membranes and with that both cecropin B and magainin 2 form characteristic two-face amphipathic helices without threonyl facets. Complementary to this, magainin 2 showed a 20% increase in the helical content compared to those of **1** and **2** (Table S1).<sup>20</sup> The results of these folding studies support our conjecture that HDMs are able to fold upon binding to phospholipid membranes, i.e. fold in a responsive manner, but do not differentiate between membrane types, i.e. fold in a non-selective fashion. Given that HDMs underpin specialized biological functions, these findings also suggest that the lack of selective folding in membranes by **1** and **2** may not necessarily lead to differential biological activities. To probe this, we performed bacterial and mammalian cell viability tests for the peptides. Specifically, **2** proved to be strongly antimicrobial, with minimum inhibitory concentrations (MICs) typical of membrane-active antibiotics, antimicrobial and hemolytic peptides (Table 1). The antimicrobial activity of this peptide at the level of individual cells was also characteristic of AMPs. The rate of cell lysis obtained from stain-dead assays using a log-phase planktonic culture of *E. coli* and *S. aureus* reached up to 80% of total cell numbers for both bacteria within the first hour of **2** treatment (Figs 2A and S3). In these assays the fluorescence emission of propidium iodide, used as a dead cell marker, is monitored by fluorescence microscopy as a function of time, which allows to relate antimicrobial activity to membranolytic activity (Fig S3). To be

effective, AMPs must lyse microbial membranes within their proteolytic life time which falls under the doubling time of bacterial cells (20-30 min).

**Table 1.** Biological activities of the peptides used in the study

Cell	peptide					
	<b>1</b>	<b>2</b>	melittin	polymyxin B	magainin 2	cecropin B
	<i>Minimum Inhibitory Concentration, <math>\mu\text{M}</math></i>					
<i>E. coli</i> (ATCC 15597)	>100	3.1	2.3±1.1	3	25	<1
<i>S. aureus</i> (ATCC 6538)	>100	15±2.5	<1	25	>50	50
<i>P. aeruginosa</i> (ATCC 27853)	>100	25	9.4±4.4	1.5	>50	1.5
<i>S. typhimurium</i> (6192)	>100	40±5	3.1	1.5	>50	1.5
<i>K. pneumoniae</i> (NCTC 5055)	>100	50	3.1	2.6±0.9	<12	1.5
<i>B. subtilis</i> (ATCC 6633)	>100	15±2.5	3.1	3.1	3.1	>50
<i>M. luteus</i> (ATCC 49732)	>100	1.5	<1	2±0.9	<1	<1
	<i>LC<sub>50</sub>, <math>\mu\text{M}</math><sup>a</sup></i>					
Human erythrocytes	>250	>250 <sup>b</sup>	<10	>250 <sup>b</sup>	>250 <sup>b</sup>	>250 <sup>b</sup>

<sup>a</sup>Concentration required to achieve 50% cell death compared to untreated cells; <sup>b</sup>≤5% hemolysis at 250  $\mu\text{M}$ .

This was consistent with the results of stain-dead assays (Figs 2A and S3). As expected, **1** showed no antimicrobial activity and none of the peptides was hemolytic (Table 1 and Fig S3). It should be noted here that red blood cells carry a weak negative charge. Therefore, we incubated the peptides with primary human dermal fibroblasts whose zwitterionic membranes may better relate to peptide folding observed in neutral reconstituted membranes (Figs 2B & C). PrestoBlue cell proliferation and viability assays in conjunction with fluorescence microscopy were used to monitor the viability of fibroblasts as a function of peptide concentration. These assays are quantitative chemical and enzymatic redox indicators of metabolically active cells. After 24-hour incubations, none of **1** and **2** was appreciably lytic to the cells.

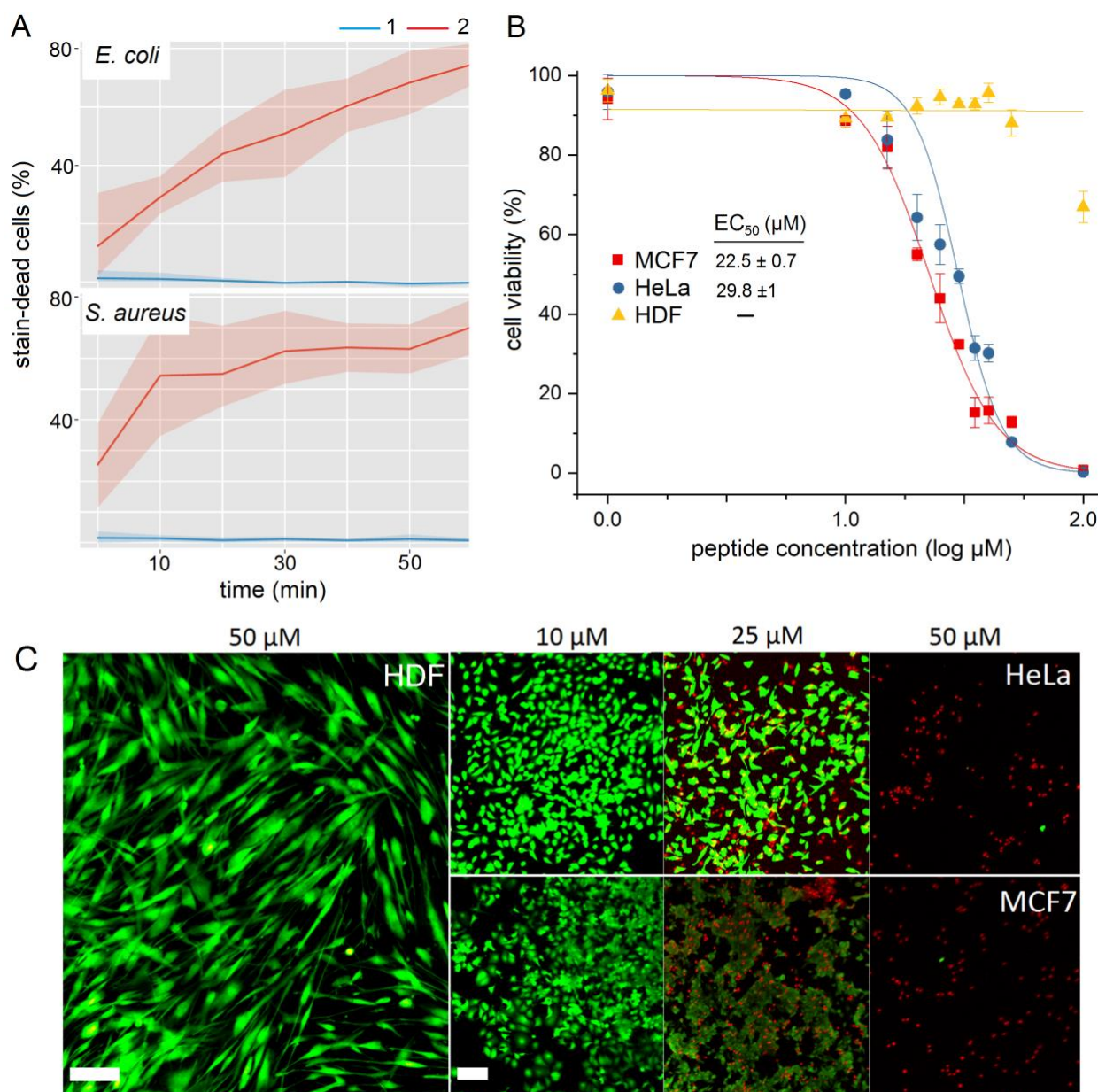


**Figure 2. Antimicrobial and anticancer activities of the helminth antibiotic template.** (A) Average numbers of stain-dead bacteria as a function of time after subtracting background numbers (buffer) for cells incubated with **1** and **2** (10  $\mu\text{M}$ ). The data represent mean values  $\pm$  s. d. (B) Dose response curves and extracted  $\text{EC}_{50}$  values for **2** on the viability of primary human dermal fibroblasts (HDF) and human cancer breast cells (MCF7) and cervical cells (HeLa). (C) Overlaid fluorescence microscopy images of HDF, HeLa and MCF7 cells following dual-colour cell viability assays after 24-h incubations with **2** at defined concentrations. Calcein AM (green) and propidium iodide (red) dyes with excitation/emission wavelengths of 495/515 nm and 543/619 nm, respectively, were used. Scale bars are 100  $\mu\text{m}$  for HDF and 70  $\mu\text{m}$  HeLa and MCF7 images.

The observed preference of **2** for strongly anionic membranes bears relevance to anticancer properties reported for AMPs.<sup>21</sup> Malignant transformation is associated with an increased exposure of anionic phospholipids on cell plasma membranes rendering them strongly anionic.<sup>22</sup> The process also disrupts membrane asymmetry, increasing variability in the curvature and architecture of the membranes, possibly resulting in better targets for ALPS motifs. These factors contribute to the putative anticancer activities of **2**. To gauge these, the peptide was incubated with human breast (MCF7) and cervical (HeLa) cancer cells. The cells display strongly anionic and heterogeneous plasma membranes that present common models for membrane permeabilization studies.<sup>23</sup> Following 24-h incubations (cell doubling time), PrestoBlue cell proliferation assays revealed appreciable cytotoxicity for **2** against both cell types at micromolar concentrations. Half maximal effective concentrations ( $EC_{50}$ ) obtained from dose response curves appeared to be within the ranges observed for anticancer agents and were also comparable for HeLa and MCF7 cells, being  $29.8 \pm 1 \mu\text{M}$  and  $22.5 \pm 0.7 \mu\text{M}$ , respectively (Figure 2B and Table 1).<sup>24, 25</sup> Together with increased membrane permeability visualised for both cell lines by fluorescence microscopy, the similar  $EC_{50}$  values suggest a generic membranolytic mechanism of action for **2** (Fig 2C). Consistent with this and with the results of antimicrobial tests, no oncolytic activity was observed for **1** against the cell lines tested at the same and higher concentrations.

Collectively, these findings suggest that **2** should exhibit a broad membranolytic activity for which the net negative charge of membranes is a defining factor. However, in marked contrast to AMPs, which fold in anionic membranes selectively, **1** and **2** showed similar folding characteristics in anionic and zwitterionic membranes. Such a discrepancy in seemingly related sequences suggest that the threonyl clusters in **1** and **2** may contribute to membrane binding with different, e.g. ALPS-like, activities. Despite the similarities in folding the peptides proved to have contrasting biological activities, which may derive from contrasting physical effects they have on membranes. To gain a better insight into what impacts **1** and **2** may have on membranes, we performed nanoscale topographic imaging on supported lipid bilayers (SLBs) using atomic force microscopy (AFM). The bilayers were prepared by

the deposition of the reconstituted membranes (the same as used for the folding studies, Fig S2) on mica substrates. In their unperturbed state, the SLBs appeared as flat surfaces to within  $\sim 0.1$  nm, which allows accurate measurements of peptide-induced pores.<sup>26</sup> These preparations also enable us to follow membrane disruption over extended areas and longer time periods.<sup>8</sup>

AFM revealed pore formation for anionic SLBs treated with **2** (Fig 3A, B). Transmembrane pores of  $30 \pm 12$  nm in diameter formed within 30 min without undergoing further changes for over an hour (Figs 3C, D and S4). Increasing peptide concentrations led to pore expansion, merging and eventually membrane removal in both anionic and zwitterionic membranes (Fig 3E, F, S4, S5). Intriguingly, poration in zwitterionic membranes appeared to be restricted to the outer leaflet of the bilayer, as the membrane was only removed over a depth of  $\sim 1$  nm, reminiscent of monolayer exfoliation (Fig S5).<sup>27</sup> This difference could be attributed to the ability of the threonyl cluster to form hydrogen bonding networks with phosphates. The cluster might interact with the surface of zwitterionic membranes as Coulombic interactions are reduced in these membranes in relation to those in anionic membranes. At increased peptide concentrations, such networks may become extensive enough to effect an interplay with cationic residues<sup>28</sup> and splay lipid tails in the outer leaflet promoting membrane exfoliation.<sup>8, 27</sup> No such effects were observed for **1** in either of the membrane types, anionic and zwitterionic, even at increased concentrations (Figs 3G, H and S6). Under the same conditions and similar concentration increases, magainin 2 formed abundant transmembrane pores in anionic membranes, with no apparent poration observed in zwitterionic membranes (Fig S5). Pores in anionic membranes formed within a similar timeframe as those of **2**, but were smaller ( $\sim 13.7 \pm 3.5$  nm) and relatively uniform in size (Fig S5).

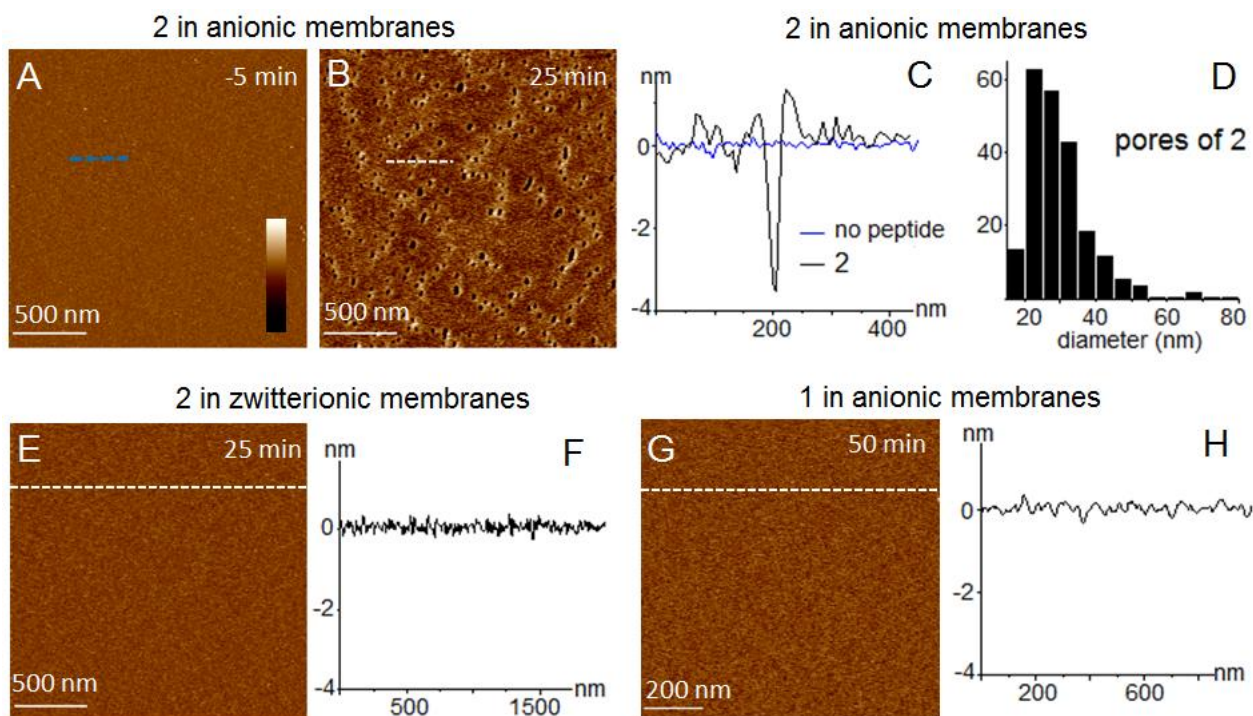


**Figure 3. In-water AFM imaging of supported lipid bilayers during peptide treatment.** Topography of anionic (A, B) and zwitterionic (E) reconstituted membranes treated with **2**. Corresponding cross sections are shown along the highlighted lines (C and F). The color scale (inset) is 6 nm. (D) Size distributions of **2** pores after the first 25 min of incubation. (G) Topography of anionic reconstituted membranes treated with **1** over 50 min. (H) A corresponding cross-section is shown along the highlighted line. Incubation conditions: 0.3  $\mu$ M peptide, pH 7.4, 20  $^{\circ}$ C.

Taken together, these results prompt a conjecture that all three faces in **2** are necessary for the activities observed. AMPs can function with just two faces – cationic and hydrophobic, while HDMs have no preference for a cationic face and arrange threonyl and hydrophobic faces instead. Both AMPs and HDMs have well-defined hydrophobic faces. To test the importance of all three faces for the activities of **2**, we designed a series of further five derivatives of the peptide (Figs 1, S7 and S8).

The first sequence in the series was converted into a helminth amphipathic helix breaker (**3**). This peptide is identical to **2** with the exception of a polar, neutral seam of glutamines introduced into the hydrophobic face (Fig 1). This seam breaks the hydrophobic face giving rise to a broken helix (Fig 1). As expected, **3** did not fold under any conditions tested and was biologically inactive (Fig S9, Tables

S1 and S2). Entirely different was the behaviour of an amphipathic antimicrobial helix **4**, which was designed by replacing the threonyl cluster of **2** with a glutamine face (Fig S7). This peptide was found to be strongly antimicrobial and non-hemolytic (Table S2). Notably, unlike **2** and similar to the naturally occurring AMPs, e.g. magainin 2 and cecropin B used in this study, the peptide folded exclusively in anionic membranes (Figs S2 and S9), and porated only anionic SLBs (Fig S10). This preference of **4** to target anionic membranes is typical of AMPs and was comparable to that of magainin 2 (Figs S2 and S5). The cytolytic selectivity of **4** was similar to that of **2**, which may be attributed to that the ratio of hydrophobic to polar residues was the same for the two peptides (Figs 1 and S7). With **1** being inactive in all biological tests performed in the study, this data provides additional support for our earlier reasoning that threonyl clusters are not necessary, but complementary, for antimicrobial activity. Searches in AMP databases revealed that threonines and serines account only for a small percentage of all residues in antimicrobial sequences, ~3% and 5.5%, respectively (Table S3).<sup>29, 30</sup> These correspond to 45% and 17% decreases, respectively, when scored against the natural abundance of these residues in all proteins (UniProt). By comparison, lysine and aspartic acids whose natural abundances are similar to those of threonine and serine show expectedly divergent abundances in antimicrobial sequences; that is, lysine proved as dominant with a 146% increase versus a 63% decrease for aspartate (Table S3). Further searches confirmed that approximately 1% of AMPs may incorporate threonyl clusters (three or more residues arranged in  $i$ ,  $i+3$  or  $i+4$  spacings).<sup>29, 30</sup> Thus, threonyl clusters are highly unusual for AMPs and are not required for antimicrobial activity. To this end, the threonyl cluster in **2** was shown to contribute to membrane binding and differential poration mechanisms. However, the question remains as to how impactful changes in the cluster itself can be for biological activity. To test this, two single mutations were introduced in **2**. One was to break the cluster by replacing the threonyl residue next to serine with an alanine, to give peptide **5**. In another, peptide **6**, the cluster was converted to a lipid-packing sensor motif, NSTST, known to increase helix sensitivity to the curvature of zwitterionic membranes.<sup>31</sup> The

folding patterns of the two peptides as well as their poration mechanisms were very similar to those of **2**, and both peptides retained the antimicrobial activity of **2** (Figs S9, S10 and Table S2). Yet, strikingly, the peptides were found to be strongly hemolytic (Table S2). This dramatic loss of selectivity stands for that the continuity of three threonyl residues in the cluster is critical for the differential activity of **2**. It is also possible that alanine in **5**, whose hemolytic activity was nearly twice that of **6**, not only breaks the cluster, but also increases hydrophobicity and helicity in it. This may bias the remaining threonyl residues to form a contiguous face with a more hydrophobic face that is composed of residues with high propensity for helix formation. Indeed, peptide **7**, in which the cluster residues were replaced by helical hydrophobic residues, was found to porate membranes indiscriminately at low concentrations and caused the complete lysis of red blood cells under 100  $\mu\text{M}$  (Figs S7-S10). The effects are characteristic of toxic peptides whose ratios of hydrophobic to polar residues are similarly high, e.g. 2:1 (Fig S7). Although individual residues in **7** have high helical propensities, the extension of its hydrophobic face is prone to mediate interfacial interlocking of peptide chains, which can lead to uncontrolled oligomerisation that is better accommodated in  $\beta$ -pleated structures.<sup>32</sup> Both  $\beta$ -sheet-type folding and amyloid-like fibrils were evident for the peptide (Figs S9 and S11).

## Conclusion

In conclusion, we have demonstrated that HDMs constitute effective structure-activity templates for designing broad spectrum antibiotics against bacterial and cancer cells. Using an archetypal HDM that exhibits no cytolytic activity, we capitalized on structural similarities between HDMs with AMPs. The amphipathic nature of HDMs was shown to pre-determine responsive and non-differential folding upon binding to membranes. Our study suggests a synergistic effect in **2** between a threonyl cluster and cationic and hydrophobic faces to deliver a preferential attack on anionic membranes. The cluster proves to regulate the cytolytic selectivity of the template. Single mutations that break the continuity of its three threonyl residues dramatically increase peptide toxicity. We therefore reason that by

contributing with a distinctive face in the amphipathic helix the threonyl cluster may facilitate selectivity in disordering lipid packing. Arguably, the structural role of the proposed template is most relevant to that of membrane-associated amphipathic helices, which also contain cationic and hydrophobic faces. For example, in the capsids of non-enveloped viruses such helices promote viral egress from endosomes into the cytoplasm by lysing endosomal membranes.<sup>33</sup> Similar to viruses, HDM amphipathic helices use endocytosis to enter cells.<sup>10</sup> However, unlike capsid helices and AMPs that tend to lyse membranes, HDMs associate with membranes to prevent endosomal acidification without causing cell death.<sup>12,13</sup> That is, the threonyl cluster of HDMs may represent a conserved motif that can specifically sense and exploit membrane surfaces and in synergy with cationic and hydrophobic faces can preferentially target anionic membranes. We have shown that this distinctive property of HDMs to sense membranes without disrupting them can be combined with poration mechanisms of AMPs to help engineer membrane responsive antibiotics. Resulting structures incorporate membrane sensing and poration properties that, to the best of our knowledge, have not been reported so far. **2** may also be functionally appropriate to underpin unexplored solutions to circumvent the resistance mechanisms of tumor and bacterial cells to oncolytic and antimicrobial peptides whose structural properties are limited to those of conventional AMPs.<sup>34, 35</sup>

## **METHODS**

**Peptide synthesis, identification and purification.** All peptides were assembled uncapped on a Wang resin in a Liberty Blue microwave peptide synthesizer (CEM Corp.) using Fmoc/Bu synthesis protocols. HBTU/DIPEA were used as coupling reagents. Following cleavage and deprotection (95% TFA, 2.5% TIS, 2.5% H<sub>2</sub>O), the peptides were purified by semi preparative RP-HPLC. The purity and identities of the peptides were confirmed by analytical RP-HPLC ( $\geq 95\%$ ) and MALDI-ToF mass spectrometry: MS [M + H]<sup>+</sup>: **1**, *m/z* 2140.5 (calc) 2144.3 (found); **2**, *m/z* 2082.6 (calc) 2084.9 (found); **3**, *m/z* 2156.5 (calc) 2160.5 (found); **4**, *m/z* 2204.7 (calc) 2207.5 (found); **5**, *m/z* 2052.6 (calc) 2054.4 (found); **6**, *m/z* 2068.6 (calc) 2072.2 (found); **7**, *m/z* 2144.8 (calc) 2146.2 (found); cecropin B – *m/z*

3834.7 (calc), 3836.7 (found); magainin 2 amide – m/z 2465.9 (calc), 2466.1 (found); melittin – m/z 2846.5 (calc), 2846.7 (found).

Analytical and semi-preparative RP-HPLC were performed on a Thermo Scientific Dionex HPLC System (Ultimate 3000) using Vydac C18 (5 $\mu$ m) columns. Runs used a 10-70% buffer B gradient over 30 mins at 1 mL/min (analytical) and 4.7 mL/min (semi-preparative), with detection at 214 and 230 nm. Buffer A and buffer B were 5% and 95% (vol/vol) aqueous CH<sub>3</sub>CN containing 0.1% TFA.

<sup>1</sup>H NMR spectra were collected at 298K with a Bruker Avance 600 (600.50 MHz) equipped with a BBI probe. An excitation sculpting pulse sequence for water suppression was used (spectral width of 12335.5 Hz and relaxation delay of 4 s). Lyophilised peptides were dissolved in mixture of water and deuterated water. Each spectrum was averaged over 128 scans.

The characterization data, RP-HPLC profiles, HRMS and NMR spectra are given in Fig S1.

**Minimum inhibitory concentrations assay.** Minimum inhibitory concentrations (MICs) were determined by broth microdilution on *P. aeruginosa*, *E. coli*, *S. aureus*, *M. luteus*, *B. subtilis*, *S. typhimurium* and *K. pneumoniae* according to the Clinical and Laboratory Standards Institute. Typically, 100  $\mu$ L of 0.5–1  $\times$  10<sup>6</sup> CFU per ml of each bacterium in Mueller Hinton media broth (Oxoid) were incubated in 96-well microtiter plates with 100  $\mu$ L of serial two-fold dilutions of the peptides (from 100 to 0  $\mu$ M) at 37 °C on a 3D orbital shaker. The absorbance was measured after peptide addition at 600 nm using a SpectraMax i3x Multi-Mode Microplate Reader (Molecular Devices). MICs were defined as the lowest peptide concentration that inhibited visible bacterial growth after 24 h at 37 °C. All tests were done in triplicate and results are summarized in Tables 1 and S2. The values that are given without standard deviations are those for which no variations were found within triplicates.

**Hemolysis assay.** Hemolysis was determined using human erythrocytes sourced commercially from Cambridge Bioscience Ltd. and used within two days. 10% (vol/vol) suspensions of human erythrocytes were incubated with peptides. The cells were rinsed four times in 10 mM phosphate buffer saline (PBS, Gibco™), pH 7.2, by repeated centrifugation and re-suspension (3 min at 3000  $\times$  g). The

cells were then incubated at room temperature for 1 h in either deionized water (fully hemolysed control), PBS, or with peptide in PBS. After centrifugation at  $10,000 \times g$  for 5 min, the supernatant was separated from the pellet, and the absorbance was measured at 550 nm using a SpectraMax i3x Multi-Mode Microplate Reader (Molecular Devices). Absorbance of the suspension treated with deionized water defined complete hemolysis. All tests were done in triplicate and results are shown in Table 1. The values given in Tables 1 and S2 correspond to concentrations needed to kill a half of the sample population (50% lysis of erythrocytes) and are expressed as median lethal concentrations –  $LC_{50}$ .

**Bacterial viability LIVE/DEAD® BacLight™ assays.** *E. coli* and *S. aureus* cultures (2 mL) were centrifuged to give a cell pellet, which was washed twice with 10 mM phosphate buffer (pH 7.4) before being reconstituted in the same buffer to give  $OD_{600nm} = 0.008$ . A 150- $\mu$ L aliquot of the solution was dispensed in an eight-well glass chamber (Ibidi) with LIVE/DEAD® BacLight™ bacterial viability kit (ThermoFisher Scientific) and left to surface-settle for 20 min. The chambers were then mounted on a confocal microscope (FV1000, Olympus) equipped with a 40x/1.3 objective lens (UPLSAPO, Olympus) and fluorescence images were acquired at different time points over 60 min at 37 °C after the addition of peptides (150  $\mu$ L, 20  $\mu$ M). SYTO®9 and PI fluorescence excitation/emission were monitored at 488/519 nm and 543/619 nm, respectively.

*Image analysis.* Individual bacteria were localised and segmented in each colour channel and then their respective mean intensities were plotted on a scatter plot. A Gaussian mixture model was used to identify the distributed populations of live and dead bacteria. Once labelled, the compromised bacteria were counted at each time point and graphed. The images were denoised using a 5x5 pixel Wiener filter and eroded by 1 pixel. Image histograms were equalised, normalised and binarised with a 0.9 threshold. Bacteria were localised using the 4-pixel connectivity of the binary images. The analysis was performed on average for  $\sim 10^3$  cells for each time point for each peptide. Each measurement was

done at least in triplicate. The data is summarised in Figs 2A and S3, and shows the number of dead bacteria as a percentage of the total number of cells (taken as 100% for each point).

**Preparation of unilamellar phospholipid vesicles.** 1,2-dilauroyl-sn-glycero-3-phosphocholine (DLPC) with 1,2-dilauroyl-sn-glycero-3-phospho-(1'-rac-glycerol) (DLPG) lipids used for vesicle construction were from Avanti Polar Lipids (Alabaster, USA). DLPC were used as mammalian model membranes, and DLPC/DLPG (3:1, molar ratios) were used as bacterial model membranes. The lipids were weighted up, dissolved in chloroform-methanol (2:1, vol/vol), dried under a nitrogen stream and then under vacuum to form a thin film. The film was hydrated in 10 mM phosphate buffer (pH 7.2) with shaking (1 h, 220 rpm) and bath sonicated for 30 min. The obtained suspension was extruded using a hand-held extruder (Avanti Polar lipids) (twenty nine times, polycarbonate filter, 0.05  $\mu\text{m}$ ) to give a clear solution of small unilamellar vesicles, whose sizes (50 nm) were confirmed by photon correlation spectroscopy.

**Photon correlation spectroscopy.** Vesicles were re-suspended to a final concentration of 1 mg/mL and were analysed on a Zetasizer Nano (ZEN3600; Malvern Instruments). Dynamic light scattering batch measurements were carried out in a low volume disposable cuvette at 25 °C. Hydrodynamic radii were obtained through the fitting of autocorrelation data using the manufacturer's software, Dispersion Technology Software (DTS version 5.10).

**Circular dichroism spectroscopy.** All CD spectra were recorded on a JASCO J-810 spectropolarimeter fitted with a Peltier temperature controller. All measurements were taken in ellipticities in mdeg and converted to molar ellipticities ( $[\theta]$ ,  $\text{deg cm}^2\cdot\text{dmol}^{-1}\text{ res}^{-1}$ ) by normalizing for the concentration of peptide bonds. Aqueous peptide solutions (300  $\mu\text{L}$ , 40  $\mu\text{M}$ ) were prepared in filtered (0.22  $\mu\text{m}$ ), 10 mM phosphate buffer, pH 7.4. CD spectra recorded in the presence of synthetic membranes are for lipid-peptide (L/P) molar ratios of 100. Data was collected with a 1 nm step, 1 sec collection time per step, and is presented as the average of 4 scans. The spectra are given in Figs S2 and S9.

**In-liquid atomic force microscopy on supported lipid bilayers.** Supported lipid bilayers were formed using a vesicle fusion method as published elsewhere.<sup>8</sup> Freshly prepared vesicles (1.5  $\mu$ L, 3mg/mL) were added to cleaved mica a pre-hydrated with buffer (70  $\mu$ L, 120 mM NaCl, 20 mM MOPS, 20 mM MgCl<sub>2</sub>). Following adsorption and incubation for 45 min, the samples were washed to remove unfused vesicles and resulting SLBs were checked to confirm they were defect free. Peptides were then introduced into a 100- $\mu$ L fluid cell (Bruker AXS, USA) where they were diluted to the final concentrations of 0.1-0.8  $\mu$ M. All imaging was performed using Peak Force Tapping<sup>TM</sup> mode on a Multimode 8 AFM system (Bruker AXS, USA) using MSNL-E cantilevers (Bruker AFM probes, USA). Images were taken at PeakForce frequency of 2 kHz, PeakForce amplitude of 10 nm and PeakForce set-point of 10-30 mV (<100 pN). Images were processed using Nanoscope analysis software (Bruker AXS, USA) or Gwyddion (<http://gwyddion.net>) for first order line-by-line background subtraction (flattening) and first-order plane fitting. The obtained images are given in Figs 3, S4-S6 and S10.

**In-liquid atomic force microscopy of fibril formation.** A 50- $\mu$ M solution of 7 was incubated in 20 mM HEPES (pH 7.4) for 2 hrs. 50  $\mu$ L of the solution was then added to freshly cleaved mica that was pre-hydrated with 70  $\mu$ L of an imaging buffer (120 mM NaCl, 20 mM MOPs, pH 7.4). Imaging was performed in Peak Force Tapping<sup>TM</sup> mode on a Multimode 8 AFM system (Bruker AXS, USA) using MSNL-E cantilevers (Bruker AFM probes, USA). Images were taken at the PeakForce frequency of 2 kHz, PeakForce amplitude of 20 nm and PeakForce set-point of 10-30 mV (<100 pN). Images were processed as in the above section. The obtained images are given in Fig S11.

**Human cell culture.** *Human dermal fibroblasts* (Invitrogen, UK) were maintained in Medium 106 supplemented with low serum growth supplement (2% v/v) and antibiotics (10  $\mu$ g/mL gentamicin; 0.25  $\mu$ g/mL amphotericin B) in 25 cm<sup>3</sup> culture flasks. The cells were incubated at 37 °C, 5% CO<sub>2</sub> and 95% air humidity. At 70-80% confluency, cells were washed with PBS to remove the unattached cells and then adhered cells were detached using TrypLE<sup>TM</sup> Express followed by trypsin neutralizer (all

from Thermo Fisher, UK). The harvested cells (of passages 6 to 9) were seeded for subsequent cellular analysis.

*HeLa* cells were cultured in Dulbecco Minimal Essential Eagle's Medium (DMEM) with GlutaMAX™, 10% heat-inactivated fetal bovine serum (FBS), 10 µg/mL gentamicin and 0.25 µg/mL amphotericin B. Cell cultures were maintained at 37°C under a humidified atmosphere of 5% CO<sub>2</sub> / 95% air. At 70-80% confluency cells were washed with PBS to remove the unattached cells and then adhered cells were detached using TrypLE™ Express followed by trypsin neutralizer (all from Thermo Fisher, UK).

*MCF7* cells were cultured in Minimal Essential Eagle's Medium (MEM) with GlutaMAX™, 1% Non-Essential Amino Acids (NEAA), 10% heat-inactivated fetal bovine serum (FBS), 10 µg/mL gentamicin and 0.25 µg/mL amphotericin B. Cell cultures were maintained at 37°C under a humidified atmosphere of 5% CO<sub>2</sub> / 95% air. At 70-80% confluency cells were washed with PBS to remove the unattached cells and then adhered cells were detached using TrypLE™ Express followed by trypsin neutralizer (all from Thermo Fisher, UK).

**Cell seeding and incubation with peptide.** The harvested cells were seeded into 96-well chambers with a density of  $2 \times 10^4$  cells per well. The cells were incubated overnight prior to peptide addition. Peptides were added in Opti-MEM media (Invitrogen, UK) to the cells. After 3-hr incubations complete media were added and cells were continuously incubated for 24 hours (total) and were then analyzed for cytotoxic effects. For quantitative PrestoBlue® analysis 96 well plate was used and qualitative cell live/dead analysis Ibidi 8-well chamber glass slides were used.

**Cytotoxicity analysis.** Cytotoxicity following peptide addition was determined by PrestoBlue®. The reagent supplied as a 10x solution was added to each well by diluting (1x) in culture medium. The cells were incubated for 30 minutes at 37 °C in 200 µL of the reagent. The fluorescence of each well was measured with a microplate reader (BMG Labtech, Germany), with 544 nm excitation and 590 nm emission filters. Standard calibration curves were generated by plotting measured fluorescence

values versus cell numbers. For cell death analysis live/dead cells were tested using calcein AM and propidium iodide dye. Cells were imaged using an inverted confocal laser scanning microscope (FV-1000, Olympus). No image processing was performed after image acquisition.

**Abundance of threonine and serine residues.** The natural percentage abundance of threonine and serine residues was taken from the UniProtKB database (<https://www.uniprot.org/statistics/Swiss-Prot>), containing a total of 559,228 sequences as of 03/2019. The percentage abundance of threonine and serine residues in helical antimicrobial peptides was calculated from AMP databases.<sup>29,30</sup> To allow direct comparisons with the HDM derivatives the calculations were performed for helical peptides lacking negative charges and exhibiting activity against both Gram positive and Gram negative bacteria. Threonyl clusters were defined as three or more threonyl residues separated at  $i$ ,  $i+3$  or  $i, i+4$  spacings in peptide sequences.

## ASSOCIATED CONTENT

**Supporting information** contains experimental notes together with additional data and figures

## AUTHOR INFORMATION

Corresponding Author

\*E-mail: max.ryadnov@npl.co.uk

ORCID

Maxim G Ryadnov: 0000-0003-4847-1154

## Notes

The authors declare no competing financial interest

## ACKNOWLEDGEMENTS

We thank Richard Thorogate for technical support; Alice Pyne and Ed Parsons for their advice on the AFM experiments, and John Warren for his advice on NMR. This work has been partly funded by the UK's Department for Business, Energy and Industrial Strategy and by the UK's BBSRC (BB/N015487/1) and EPSRC (EP/M028100/1).

## REFERENCES

1. Gouaux, E. (1997) Channel-forming toxins: tales of transformation. *Curr. Opin. Struct. Biol.* 7, 566-573.
2. Hotez, P. J., Brindley, P. J., Bethony, J. M., King, C. H., Pearce, E. J., and Jacobson, J. (2008) Helminth infections: the great neglected tropical diseases. *J. Clin. Invest.* 118, 1311–1321.
3. Zasloff, M. (2002) Antimicrobial peptides of multicellular organisms. *Nature* 415, 389–395.
4. Yeung, A. T., Gellatly, S. L., and Hancock, R. E. (2011) Multifunctional cationic host defence peptides and their clinical applications. *Cell Mol. Life Sci.* 68, 2161-2176.
5. Fjell, C. D., Hiss, J. A., Hancock, R. E., and Schneider, G. (2011) Designing antimicrobial peptides: form follows function. *Nat. Rev. Drug Discov.* 11, 37-51.
6. Shai, Y. (2002) Mode of action of membrane active antimicrobial peptides. *Biopolymers* 66, 236–248.
7. Rakowska, P. D. et al. (2013) Nanoscale imaging reveals laterally expanding antimicrobial pores in lipid bilayers. *Proc. Natl. Acad. Sci. USA* 110, 8918-8923.
8. Pyne, A. et al. (2017) Engineering monolayer poration for rapid exfoliation of microbial membranes. *Chem. Sci.* 8, 1105-1115.
9. Needham, B. D., and Trent, M. S. (2013) Fortifying the barrier: the impact of lipid A remodeling on bacterial pathogenesis. *Nat. Rev. Microbiol.* 11, 467-481.
10. Robinson, M. W., Donnelly, S., and Dalton, J. P. (2013) Helminth defence molecules – immunomodulators designed by parasites! *Front. Microbiol.* 4, 296.
11. Robinson, M. W. et al. (2011) A family of helminth molecules that modulate innate cell responses via molecular mimicry of host antimicrobial peptides. *PLoS Pathog.* 7, e1002042.
12. Robinson, M. W. et al. (2012) A helminth cathelicidin-like protein suppresses antigen processing and presentation in macrophages via inhibition of lysosomal vATPase. *FASEB J* 26, 4614–4627.

13. Alvarado, R., To, J., Lund, M. E., Pinar, A., Mansell, A., Robinson, M. W., O'Brien, B. A., Dalton, J. P., and Donnelly, S. (2017) The immune modulatory peptide FhHDM-1 secreted by the helminth *Fasciola hepatica* prevents NLRP3 inflammasome activation by inhibiting endolysosomal acidification in macrophages. *FASEB J* 31, 85-95.
14. Thivierge, K., Cotton, S., Schaefer, D. A., Riggs, M. W., To, J., Lund, M. E., Robinson, M. W., Dalton, J. P., and Donnelly, S. M. (2013) Cathelicidin-like Helminth Defence Molecules (HDMs): absence of cytotoxic, antimicrobial and anti-protozoan activities imply a specific adaptation to immune modulation. *PLoS Negl. Trop. Dis.* 7, e2307.
15. Hayouka, Z., Bella, A., Stern, T., Ray, S., Jiang, H., Grovenor, C. R. M., and Ryadnov, M. G. (2017) Binary encoding of random peptide sequences for selective and differential antimicrobial mechanisms. *Angew. Chem. Int. Ed.* 56, 8099-8103.
16. Matsuzaki, K., Yoneyama, S., and Miyajima, K. (1997) Pore formation and translocation of melittin. *Biophys. J* 73, 831–838.
17. Hallock, K. J., Lee, D.-K., Omnaas, J., Mosberg, H. I., and Ramamoorthy, A. (2002) Membrane composition determines pardaxin's mechanism of lipid bilayer disruption. *Biophys J* 83, 1004-1013.
18. Doucet, C. M., Esmery, N., de Saint-Jean, M., and Antonny, B. (2015) Membrane curvature sensing by amphipathic helices is modulated by the surrounding protein backbone. *PLoS One* 10, e0137965.
19. Ballesteros, J. A., Deupi, X., Olivella, M., Haaksma, E. E., and Pardo, L. (2000) Serine and threonine residues bend alpha-helices in the  $\chi(1) = g(-)$  conformation. *Biophys. J* 79, 2754-2760.
20. Morrisett, J. D., Jackson, R. L., and Gotto, A. M., Jr. (1977) Lipid-protein interactions in the plasma lipoproteins. *Biochim. Biophys. Acta*, 472, 93-133.

21. Gaspar, D., Veiga, A. S., and Castanho, M. A. R. B. (2013) From antimicrobial to anticancer peptides. A review. *Front. Microbiol.* 4, 294.
22. Ran, S., Downes, A., and Thorpe, P. E. (2002) Increased exposure of anionic phospholipids on the surface of tumour blood vessels. *Cancer Res.* 62, 6132-6140.
23. Chen, B. et al. (2016) Targeting negative surface charges of cancer cells by multifunctional nanoprobe. *Theranostics* 6, 1887-1898.
24. Wang, C., Dong, S., Zhang, L., Zhao, Y., Huang, L., Gong, X., Wang, H., and Shang, D. (2017) Cell surface binding, uptake and anticancer activity of L-K6, a lysine/leucine-rich peptide, on human breast cancer MCF-7 cells. *Sci Rep.* 7, 8293.
25. Florento, L., Matias, R., Tuano, E., Santiago, K., dela Cruz, F., and Tuazon, A. (2012) Comparison of cytotoxic activity of anticancer drugs against various human tumor cell lines using in vitro cell-based approach. *Int. J Biomed. Sci.* 8, 76-80.
26. Mingeot-Leclercq, M.-P., Deleu, M., Brasseur, R., and Dufrêne, Y. F. (2008) Atomic force microscopy of supported lipid bilayers. *Nat. Protoc.* 3, 1654–1659.
27. Pfeil, M. P. et al. (2018) Tuneable poration: host defense peptides as sequence probes for antimicrobial mechanisms. *Sci Rep.* 8, 14926.
28. Cerasoli, E., Ravi, J., Gregor, C., Hussain, R., Siligardi, G., Martyna, G., Crain, J., and Ryadnov, M. G. (2012) Membrane mediated regulation in free peptides of HIV-1 gp41: minimal modulation of the hemifusion phase. *Phys. Chem. Chem. Phys.* 14, 1277-1285.
29. Wang, G. et al. (2009) APD2: the updated antimicrobial peptide database and its application in peptide design. *Nucleic Acids Res.* 37, D933–D937.

30. Eliseev, I. E, Terterov, I. N, Yudenko, A. N., and Shamova, O. V. (2018) Linking sequence patterns and functionality of alpha-helical antimicrobial peptides. *Bioinformatics*. doi: 10.1093/bioinformatics/bty1048
31. Mesmin, B., Drin, G., Levi, S., Rawet, M., Cassel, D., Bigay, J. and Antony, B. (2007) Two lipid-packing sensor motifs contribute to the sensitivity of ArfGAP1 to membrane curvature. *Biochemistry* 46, 1779-1790.
32. Kashchiev, D. (2018) Growth probability and formation time of the individual Oosawa-Kasai protein fibril. *Phys. Rev. E* 98, 012412.
33. Wiethoff, C. M., Wodrich, H., Gerace, L., and Nemerow, G. R. (2005) Adenovirus protein VI mediates membrane disruption following capsid disassembly. *J Virol.* 79, 1992-2000.
34. Ishikawa, K., Medina, S. H., Schneider, J. P., and Klar, A. J. S. (2017) Glycan alteration imparts cellular resistance to a membrane-lytic anticancer peptide. *Cell Chem. Biol.* 24, 149-158.
35. Ryan, L. et al. (2013) Anti-antimicrobial peptides: coiled-coil-mediated host defense antagonism. *J Biol. Chem.* 288, 20162-20172.

# Helminth defense molecules as design templates for membrane-active antibiotics

*Katharine Hammond, Helen Lewis, Nilofar Faruqi, Craig Russell, Bart W Hoogenboom and  
Maxim G Ryadnov*

## Tables and Figures

**Table S1.** Percent helicity for the peptides used in the study<sup>20</sup>

peptide	% helicity in unilamellar vesicles	
	zwitterionic	anionic
1	43.1	47.7
2	32.3	41.7
3	-	-
4	-	44.9
5	18.0	40.1
6	11.8	42.7
7	-	-
magainin 2	-	62.7
cecropin B	-	41.9

**Table S2.** Biological activities of the peptides used in the study

Cell	peptide			
	3	4	5	6
	<i>Minimum Inhibitory Concentration, <math>\mu\text{M}</math></i>			
<i>E. coli</i> (ATCC 15597)	>100	3.1	3.1	2.08 ± 0.9
<i>S. aureus</i> (ATCC 6538)	>100	>50	5.2 ± 1.8	>50
<i>P. aeruginosa</i> (ATCC 27853)	>100	3.1	3.1	2.08 ± 0.9
<i>S. typhimurium</i> (6192)	>100	20.8 ± 7.2	16.7 ± 7.2	16.7 ± 7.2
<i>K. pneumoniae</i> (NCTC 5055)	>100	12.5	12.5	25
<i>B. subtilis</i> (ATCC 6633)	>100	4.2 ± 1.8	4.7 ± 2.7	4.2 ± 1.8
<i>M. luteus</i> (ATCC 49732)	>100	<1	1.05 ± 0.44	1.05 ± 0.44
	<i>LC<sub>50</sub>, <math>\mu\text{M}</math></i>			
Human erythrocytes	>250	>250 <sup>a</sup>	<<250 <sup>b</sup>	<<250 <sup>c</sup>

<sup>a</sup>≤5%hemolysis; <sup>b</sup>72±16% and <sup>c</sup>43±7% of all cells were lysed at 250  $\mu\text{M}$ .**Table S3.** Comparative abundance of amino acids in AMPs

Amino acid	Natural abundance, % <sup>a</sup>	Abundance in AMPs, % <sup>b</sup>	Relative abundance in AMPs, % <sup>c</sup>
Ala	8.2	9.6	17
Arg	5.5	5.8	5.5
Asn	4	2.6	-35
Asp	5.4	2.0	-62.9
Cys	1.3	1.35	3.8
Gln	3.9	2.7	-30.7
Glu	6.7	2.6	-61.2
Gly	7	9.9	41.4
His	2.2	2.5	13.6
Ile	5.9	7.6	28.8
Leu	9.6	11.0	14.5
Lys	5.8	14.3	146.5
Met	2.4	1.2	-50
Phe	3.8	5.2	36.8
Pro	4.7	2.8	-40.4
Ser	6.6	5.5	-16.7
Thr	5.3	2.9	-45.2
Trp	1	2.1	110
Tyr	2.9	1.3	-55.2
Val	6.8	6.9	1.5

<sup>a</sup>in all proteins calculated for the total of 559,228 entries in UniProt<sup>b</sup>sourced from helical antimicrobial sequences in AMP databases<sup>29,30</sup><sup>c</sup>calculated as follows:  $\frac{\text{abundance in AMPs}}{\text{natural abundance}} \times 100 - 100\%$

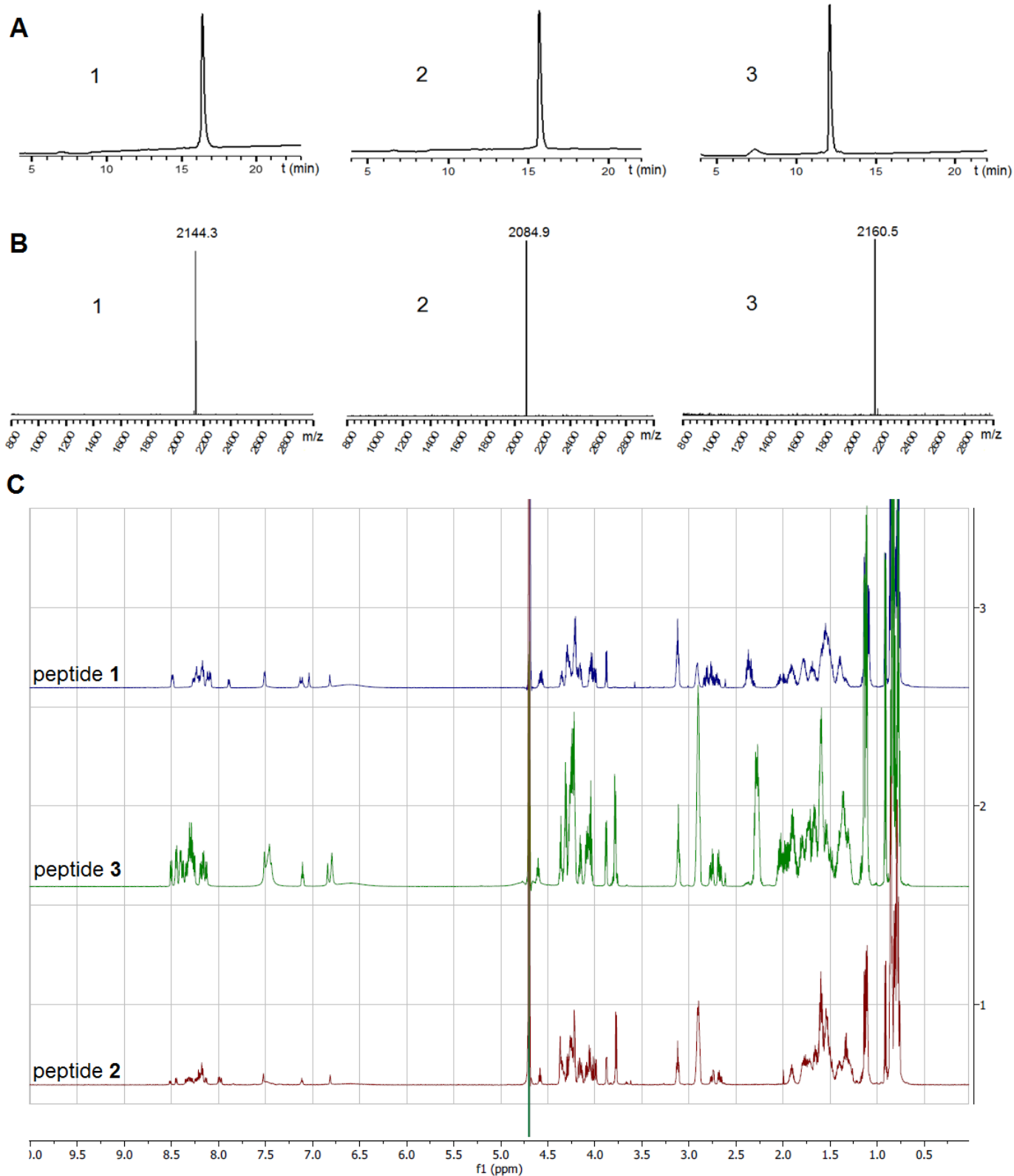


**Fig S1. Peptide characterization.** (A) RP-HPLC profiles recorded at 230 nm, (B) MALDI-ToF mass spectrometry spectra and (C) raw  $^1\text{H}$  NMR spectra for purified helminth-derived peptides used in the study.

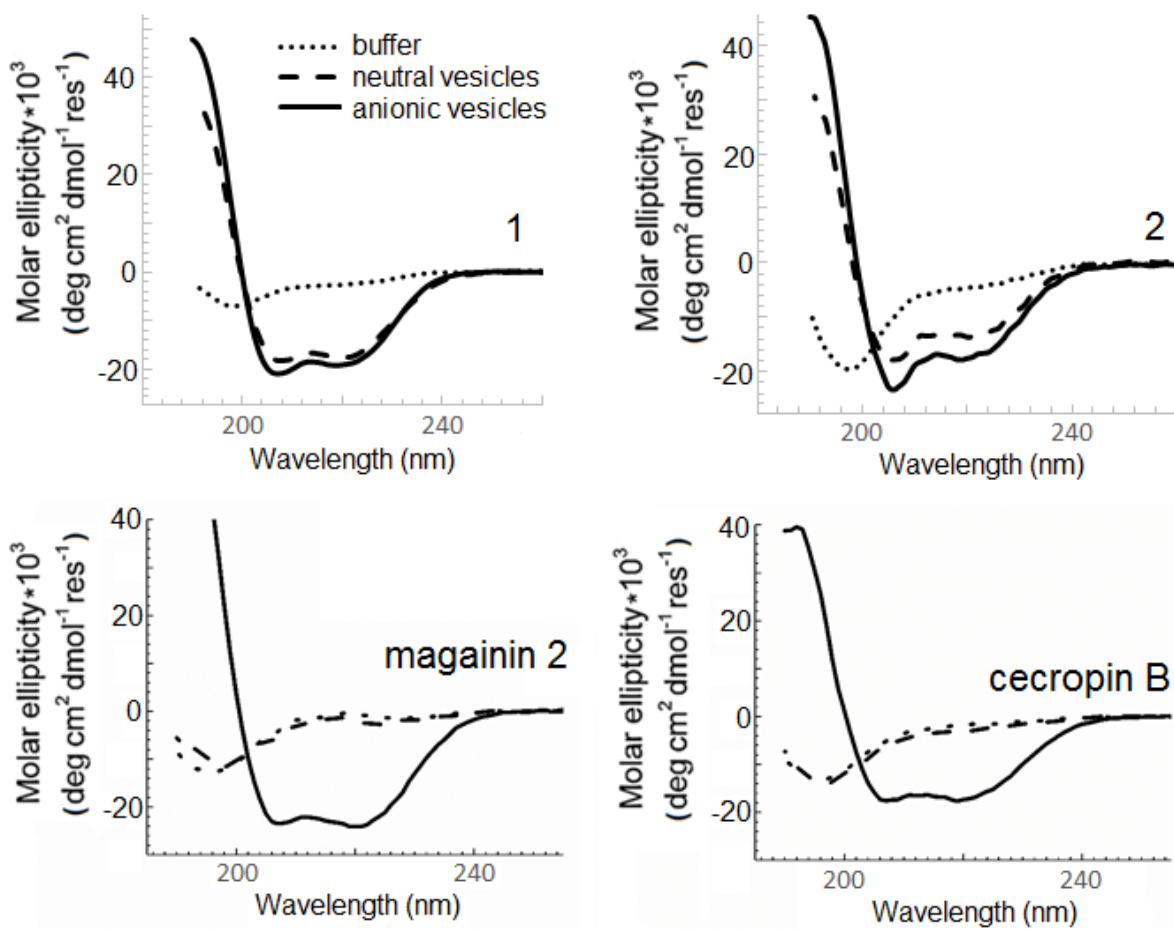


**Fig. S2. Peptide folding.** CD spectra for peptides in solution (10 mM, phosphate buffer) and in neutral (DLPC) and anionic (DLPC/DLPG at 3:1 molar ratio) vesicles. Peptides were at 40  $\mu$ M, at L/P 100 molar ratios.

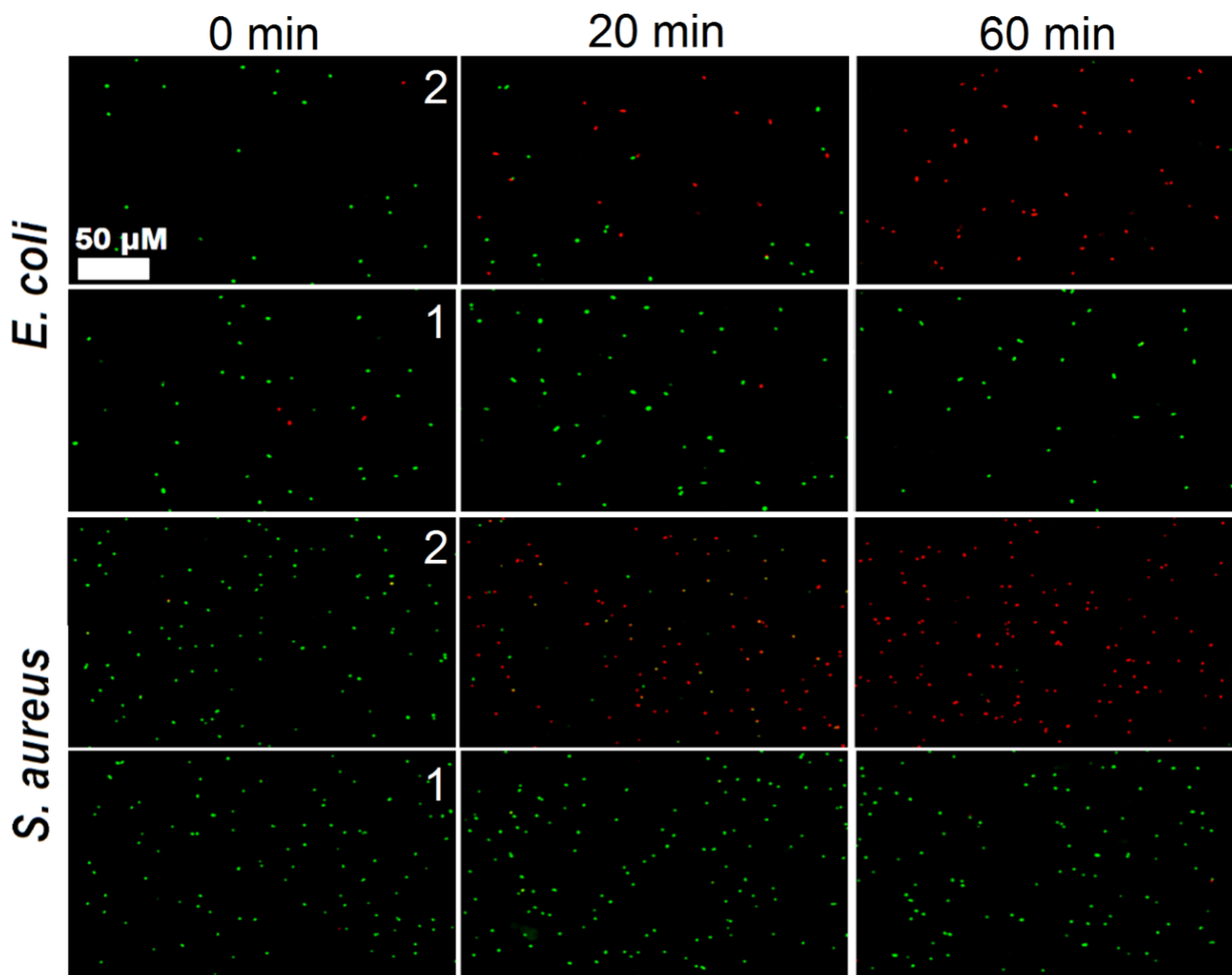


**Fig. S3. Antimicrobial kinetics of studied peptides.** Overlaid fluorescence microscopy images of bacterial cells treated with **1** and **2** at 10  $\mu\text{M}$ . The images were taken following dual-color LIVE/DEAD<sup>®</sup> BacLight<sup>™</sup> bacterial viability assays, with SYTO<sup>®</sup>9 (green) and propidium iodide (red) used to dye live and dead cells, respectively.

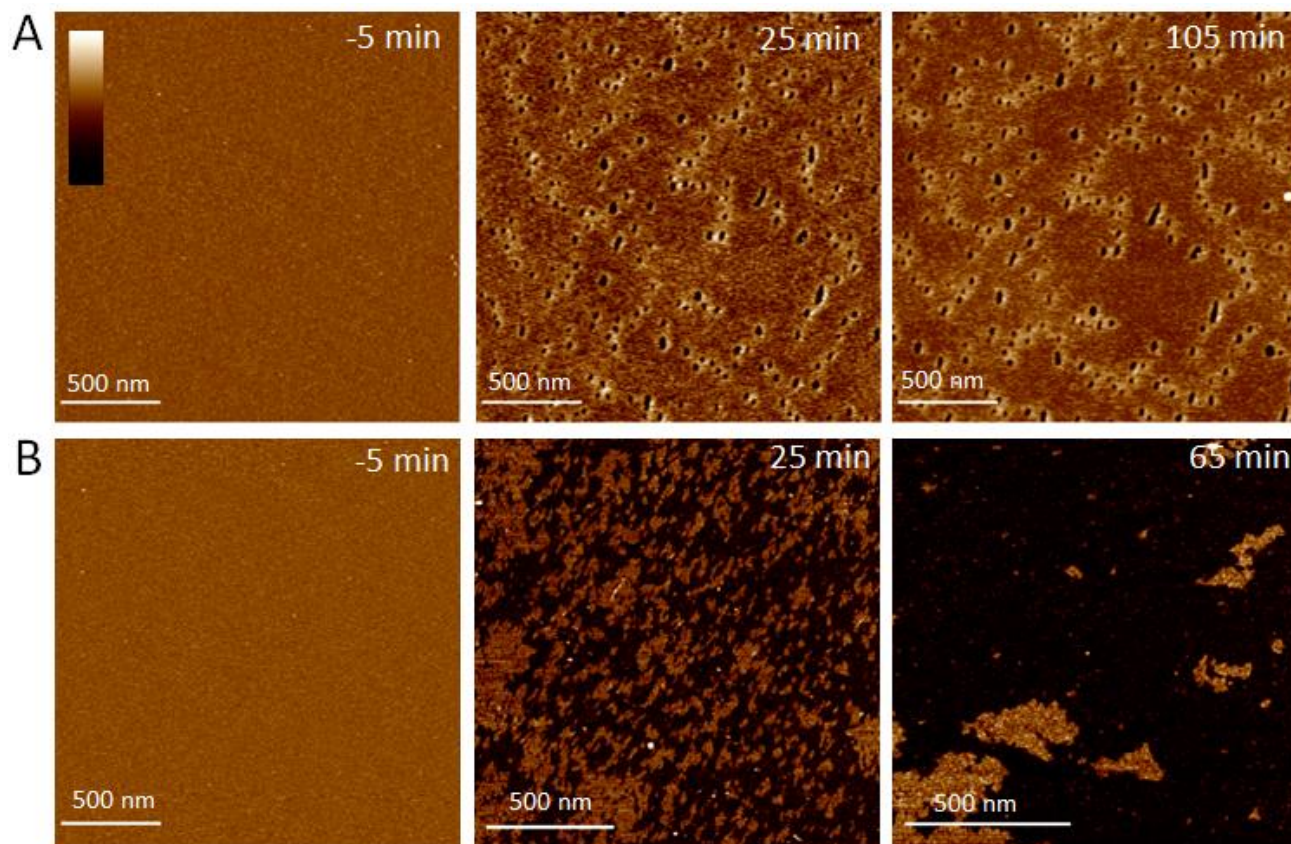


**Fig. S4. In-water AFM imaging of supported lipid bilayers treated with 2.** Topography of anionic reconstituted membranes treated with **2**. The color scale (inset) is 6 nm. Incubation conditions: peptide at 0.3 μM (**A**) and 0.8 μM (**B**), pH 7.4, 20 °C. Note: for consistency, the first two images (from left) are the same as in Fig 3A.

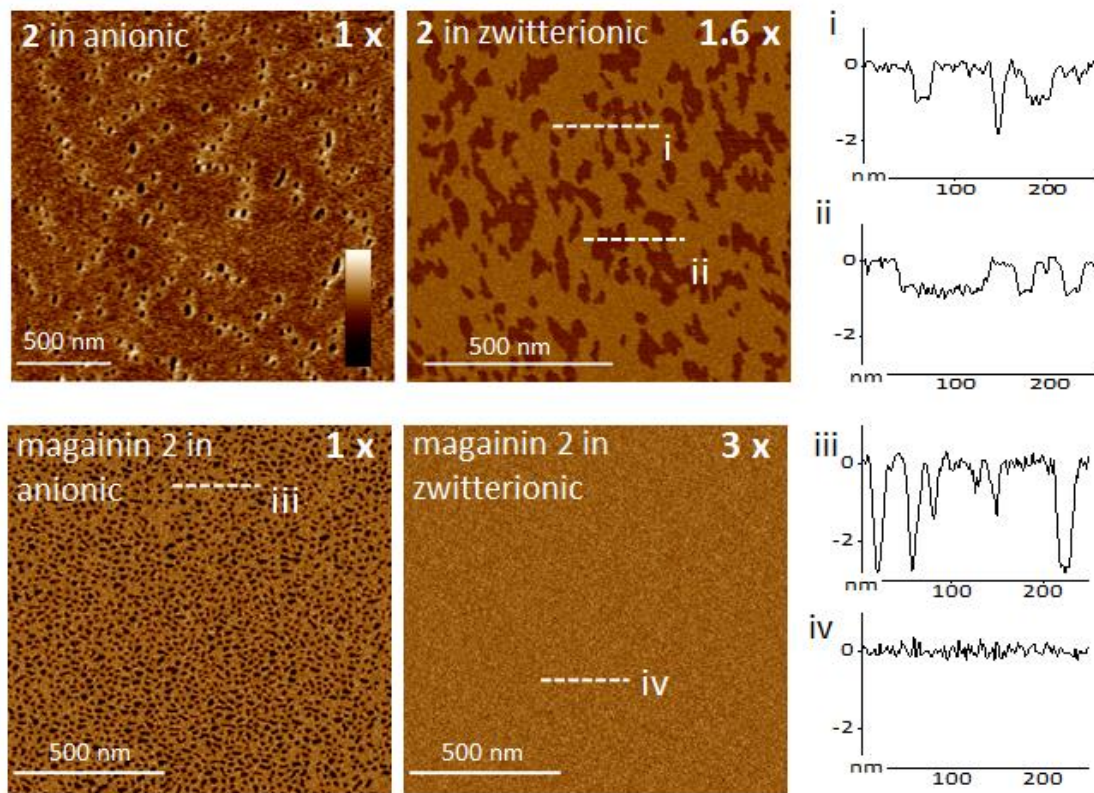


**Fig. S5. In-water AFM imaging of supported lipid bilayers during peptide treatment.** Topography images of reconstituted membranes treated with peptides as labelled in the images. Pore formation peptide concentration (1x) at 0.3  $\mu\text{M}$  and 0.1  $\mu\text{M}$  for **2** and magainin 2, respectively. Cross sections are given along the highlighted lines (i-iv). The color scale (inset) is 6 nm. All images are taken at 25 min time points.

Notes: for consistency, the upper left image in B is the same as in Figs 3A and S4; the upper right image is for **2** at 1.6 the concentration used in Fig 3E.

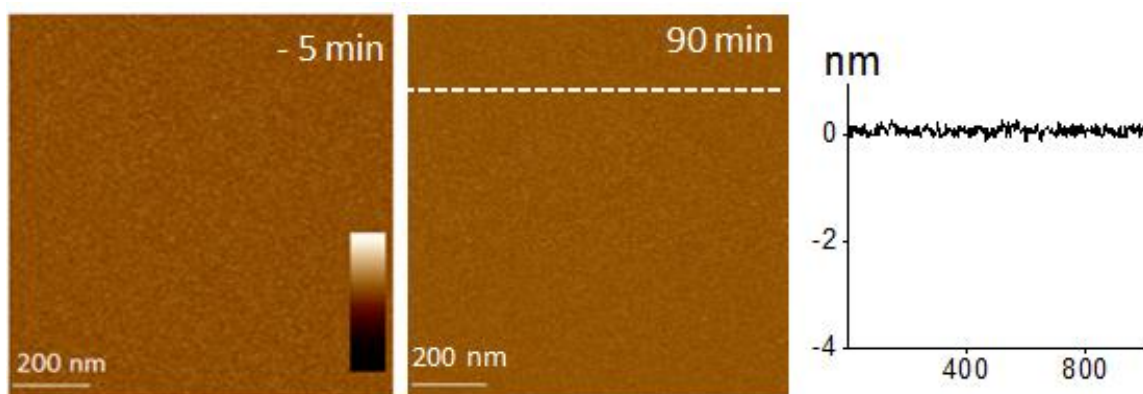


**Fig. S6. In-water AFM imaging of supported lipid bilayers during peptide treatment.** Topography of zwitterionic reconstituted membranes treated with **1** at 0.8  $\mu\text{M}$ . The color scale (inset) is 6 nm. The cross section is given along the highlighted line.

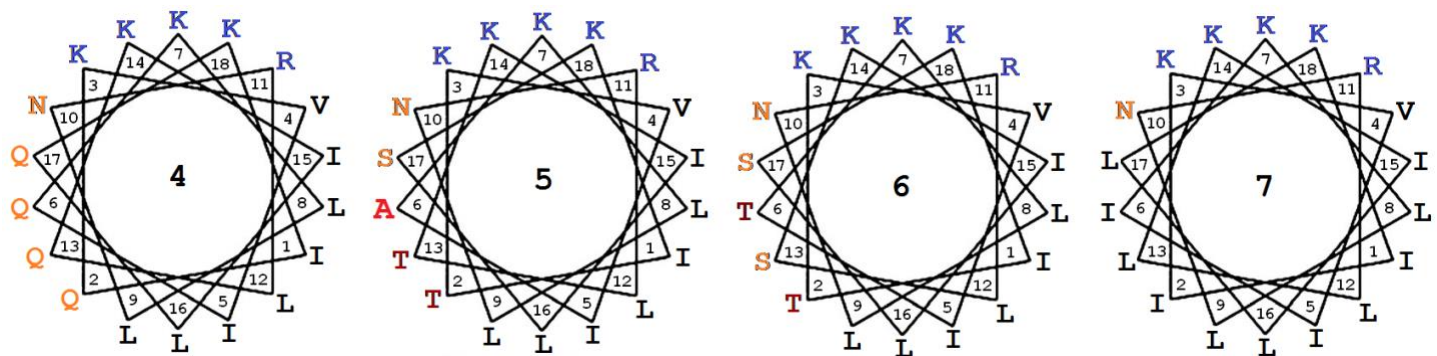


**Fig. S7. Helminth antibiotic template derivatives.** Peptide sequences configured onto helical wheels with 3.6 residues per turn. Cationic, alanine and neutral polar residues are in blue, red and orange, respectively.

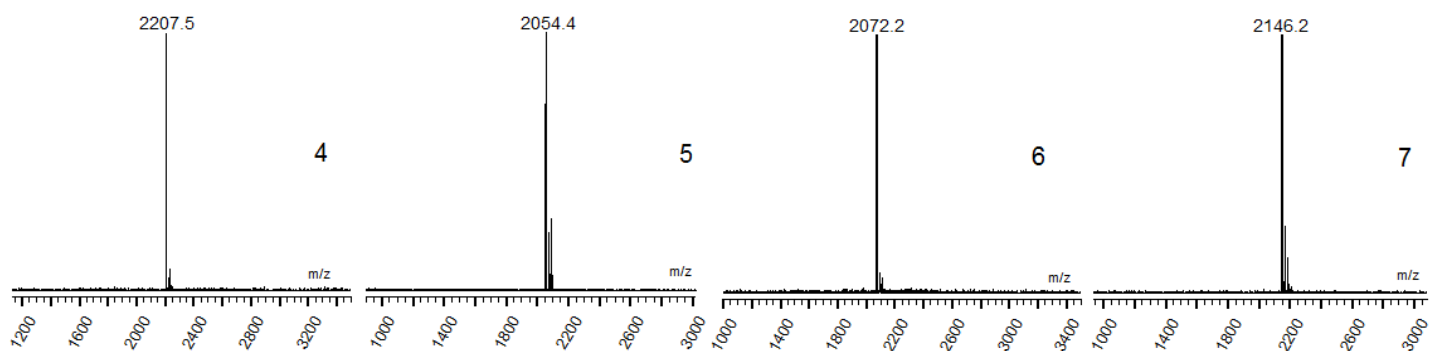


**Fig S8. Characterization of helminth antibiotic template derivatives.** MALDI-ToF mass spectrometry spectra for purified helminth-derived mutant peptides used in the study.

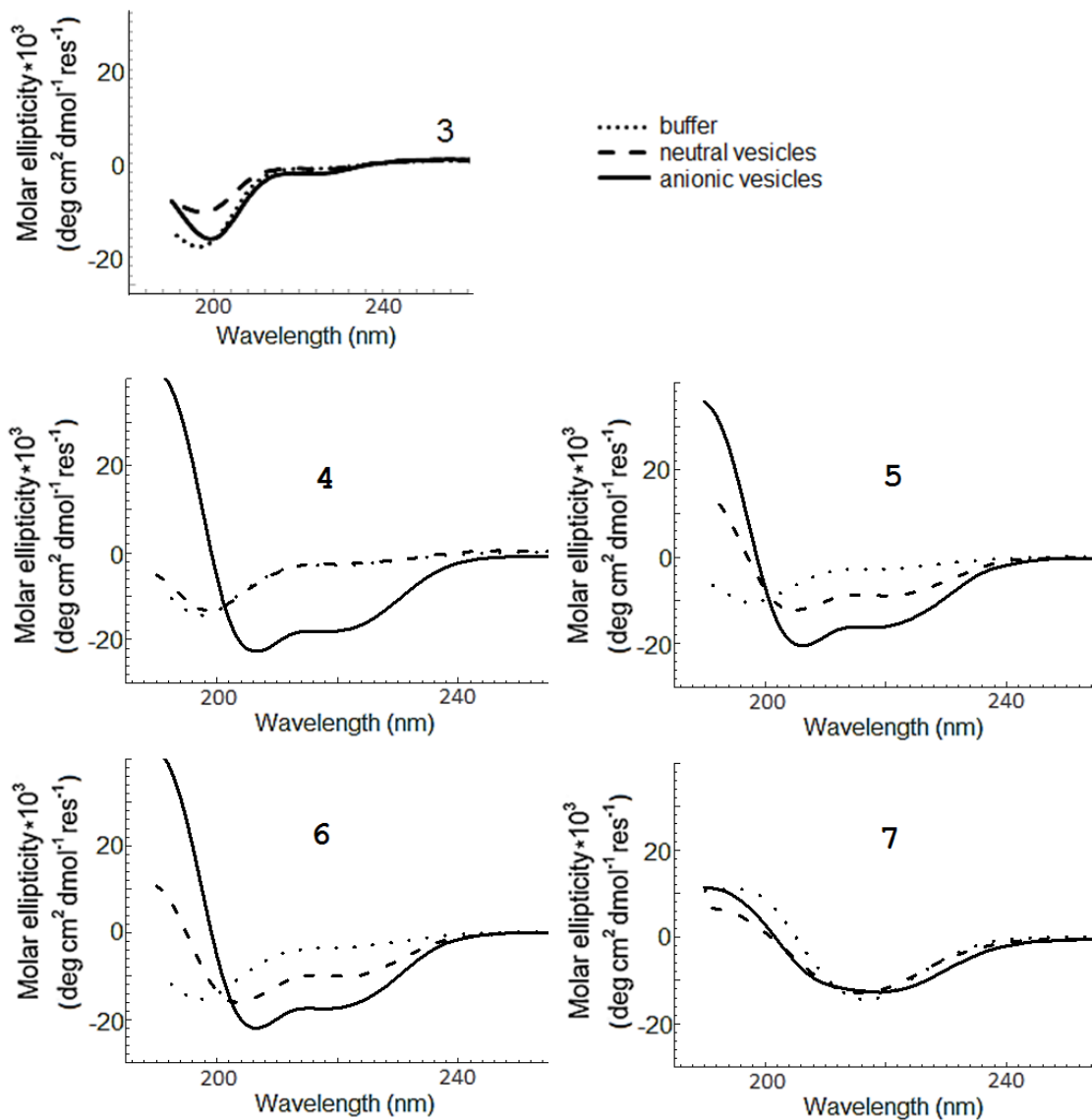


**Fig. S9. Peptide folding.** CD spectra for peptides in solution (10 mM, phosphate buffer) and in neutral (DLPC) and anionic (DLPC/DLPG at 3:1 molar ratio) vesicles. Peptides were at 40  $\mu$ M, at L/P 100 molar ratios.

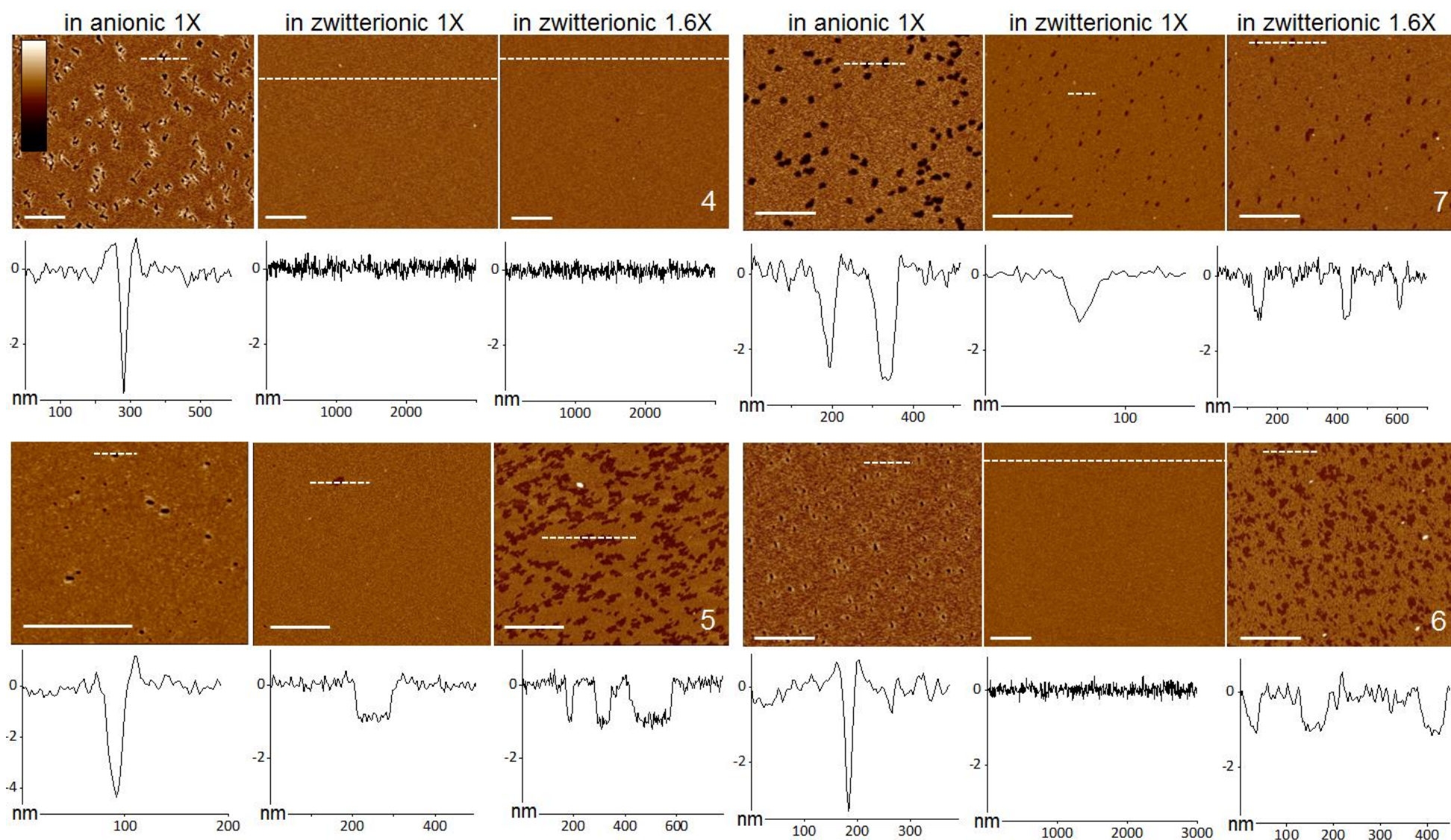


**Fig. S10. In-water AFM imaging of supported lipid bilayers during peptide treatment.** Topography images of reconstituted membranes treated with peptides as labelled in the images. Pore formation peptide concentration (1x) at  $0.3 \mu\text{M}$ . Cross sections are given along the highlighted lines under each image. The color scale (inset in the first image) is 6 nm. All scale bars are 500 nm. All images are taken at 30 min time points.

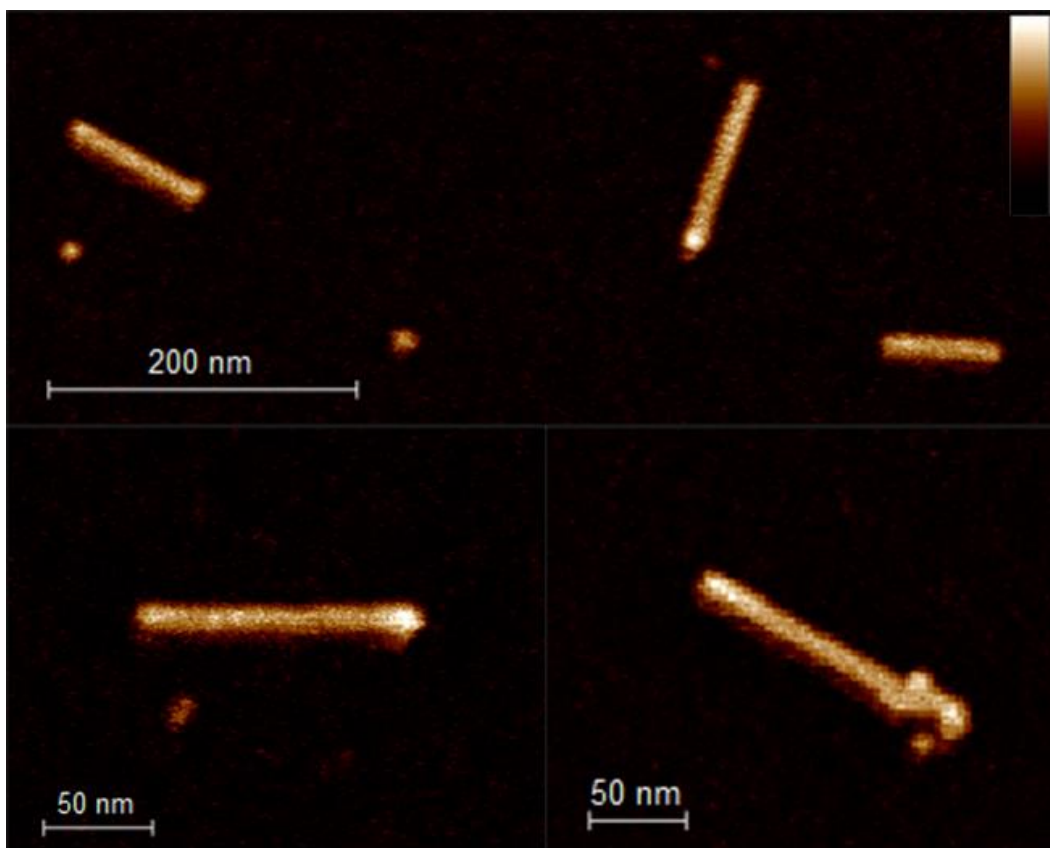


**Fig. S11. In-water AFM imaging of fibril formation.** Topography images of 7. The color scale is 6 nm.